THEMIS, BBSO, MDI AND TRACE OBSERVATIONS OF A FILAMENT ERUPTION

Contarino[1] L., Romano[1] P., Yurchyshyn[2] V.B., Zuccarello[1] F.
[1] *Dipartimento di Fisica ed Astronomia, Universitá di Catania - Via S.Sofia, 78 - 95125 - Catania, Italy*
[2] *Big Bear Solar Observatory, Big Bear City, CA 92314, U.S.A.*

March 18, 2003

Abstract. We describe a filament destabilization which occurred on May 5, 2001 in NOAA AR 9445, before a flare event. The analysis is based on $H\alpha$ data acquired by THEMIS operating in IPM mode, $H\alpha$ data and magnetograms obtained at the Big Bear Solar Observatory, MDI magnetograms and 171 Å images taken by TRACE. Observations at 171 Å show that $\sim$ 2.5 hours before the flare peak, the western part of the EUV filament channel seems to split into two parts. The bifurcation of the filament in the $H\alpha$ line is observed to take place $\sim$ 1.5 hours before the flare peak, while one thread of the filament erupts $\sim$ 10 minutes before the peak of the flare. Our analysis of longitudinal magnetograms shows the presence of a knot of positive flux inside a region of negative polarity, which coincides with the site of filament bifurcation. We interpret this event as occurring in two-steps: the first step, characterized by the appearance of a new magnetic feature and the successive reconnection in the lower atmosphere between its field lines and the field lines of the old arcade sustaining the filament, leads to a new filament channel and to the observed filament bifurcation; the second step, characterized by the eruption of part of the filament lying on the old PIL, leads to a second reconnection, occurring higher in the corona.

Keywords: Sun: filaments - flare - reconnection

1. Introduction

Filaments, or prominences when observed at the limb, beeing cool, dense chromospheric matter supported by magnetic fields in the lower corona, are optimally seen in the $H\alpha$ line, where they appear as dark, long and narrow structures.
Observations indicate that filaments form above the polarity inversion line (PIL) of photospheric magnetic fields and that changes in their magnetic field configuration may be closely related to energetic events like flares and coronal mass ejections (Tandberg-Hanssen, 1995; Martens and Kuin, 1989; Smith, Hildner, and Kuin, 1992).
Some authors (Antiochos and Klimchuk, 1991; Antiochos, Dahlburg, and Klimchuk, 1994) proposed that filament formation in a magnetic arcade is due, initially, to shearing of the field lines when footpoints move parallel to the neutral line, with the consequent formation of a

dip in the central part of the arcade. Successively, a radiatively driven instability causes chromospheric evaporation and plasma cooling in the dip region.

Recently Martens and Zwaan (2001), presented a model of the origin and evolution of filaments, based on convergence and cancellation of the photospheric magnetic field (see also Amari et al., 2003).

As far as the activation and eruption phase of filaments is concerned, several authors suggested that this phase may be induced by temporally consecutive phases such as occur during magnetic flux emergence with subsequent reconnection (Heyvaerts, Priest, and Rust, 1977) or during gradual changes of the magnetic topology surrounding the filament which lead to a catastrophic loss of equilibrium (Gaizauskas, 1989; Priest & Forbes, 2002).

Recently, Kim et al. (2001) described the eruption of a filament showing a rapid change in its connectivity in terms of a pre-eruption reconnection occurring in the low atmosphere.

In this context, observations of the morphology, evolution and dynamic processes in $H\alpha$ filaments, together with analysis of changes in the photospheric magnetic field, are needed to understand coronal filament destabilization and associated events.

In this paper we describe the activation of a filament in NOAA AR 9445 on May 5 2001, which was associated with a solar flare. We have examined images acquired by the Telescope Heliographique pour l'Etude du Magnetisme et des Instabilites Solaires (THEMIS) along the $H\alpha$ line profile during the pre-flare phase, $H\alpha$ images and longitudinal magnetograms taken at the Big Bear Solar Observatory (BBSO), full-disk MDI magnetograms, coronal images taken by the Transition Region and Coronal Explorer (TRACE) at 171 Å, during the pre-flare (18:07 - 18:19 UT), the peak (18:20 UT) and the main phase (18:21 - 18:34 UT)(Fig. 1).

The BBSO data include high resolution $H\alpha$ images and VMG magnetograms as well as full disk BBSO $H\alpha$ images and a GONG magnetogram.

2. Observations and Data Reduction

2.1. Characteristics of the Instruments

In the following we give a short description of the characteristics of the instruments used to acquire the data for this analysis.

- IPM

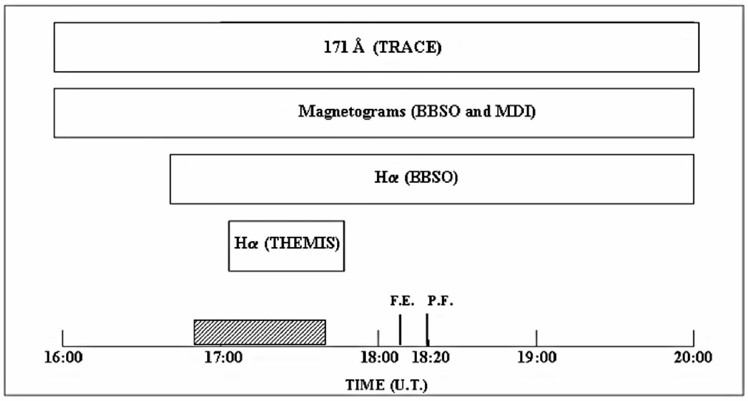

Figure 1. Time table showing data coverage from different instruments on May 5, 2001, between 16:00 and 20:00 UT. The hatched rectangle indicates the time interval of filament bifurcation as observed in the $H\alpha$ line. F.E. marks the time of filament eruption and P.F. is the time of peak of the flare.

The Italian Panoramic Monochromator on THEMIS consists of a Fabry-Perot interferometer in series with a birefringent filter (UBF). IPM obtains narrow-band (full width at half maximum=21.5 mÅ) monochromatic images with high spatial (0.2 arcsec), spectral resolution ($\lambda/\Delta\lambda \sim 256$), and with dimension of 51 $\times$ 51 arcsec. The acquisition system of IPM is formed by two CCD cameras cooled by Peltier cells with water circulation. A CCD camera obtains several images (max rate is 20 images per minute) in different spectral points along the observed line, while the second CCD camera acquires images in the continuum of the observed line (Cavallini, 1998).

- BBSO

High resolution BBSO Hα images are obtained by the 65-cm reflector, with a 0.25 Å bandpass Zeiss filter and an OSL 12 bit camera. The cadence is 30 sec with 0.3 arcsec pixel resolution. The field of view is 200 $\times$ 200 arcsec. The data, corrected for flat field and dark current, cover the period between 16:40 - 20:00 U.T.

High resolution, line-of-sight BBSO magnetograms (Varsik, 1995) are obtained by the 25-cm refractor. The pixel resolution is 0.5 arcsec, and the time cadence about 1 min. The temporal integration of each image is 4 sec and the field of view is 270 $\times$ 202 arcsec. The magnetograms are available for the time period between 16:00 and 20:00 U.T.

- MDI

The MDI instrument uses a refracting telescope (with the primary diameter of 12.5 cm) to feed sunlight through a cascade of filters onto a CCD camera (1024 $\times$ 1024 pixels and pixel size of $21\mu m$). Two tunable Michelson interferometers define a 94 mÅ bandpass that can be tuned across the Ni I 6768 Å solar absorption line. The line-of-sight magnetograms are constructed by measuring the Doppler shift separately in right and left circularly polarized light. The difference between these two signals is proportional to the magnetic flux density.
We used magnetograms taken between 16:00 UT on May 4 and 22:00 UT on May 5, with a spatial resolution of 4 arcsec and a temporal cadence of $\sim$ 30 min.

- TRACE

TRACE telescope uses three normal-incidence coatings for EUV imagery and one for UV on corresponding quadrants of the primary and secondary mirrors. A lumigen coated 1024 $\times$ 1024 CCD detector collects images over an 8.5 $\times$ 8.5 arc minute field of view (0.5 arcsec pixels) (Tarbell et al., 1994; Handy et al., 1999).
The instrument collects images of the solar plasma with one arcsec spatial resolution at the following wavelengths : 171 Å, 195 Å, 284 Å, 1216 Å, 1550 - 1700 Å and white light.
We used a sequence of TRACE images (about 350 frames) taken at 171 Å between 13:00 and 20:00 UT. All the TRACE images used in our analysis are 512 $\times$ 512 pixels, with a pixel size of 1 arcsec. The raw data have been processed using Solar SoftWare routines to correct images by means of subtraction of the pedestal and dark current, as well as to correct for radiation spikes and hot pixels.
All the images have been normalized, corrected for solar rotation and coaligned.

2.2. THEMIS Data Reduction

THEMIS data consist of a sequence of images acquired along the $H\alpha$ spectral line centered at $\lambda = 6562.8$Å.
The sequence refers to one end of the filament inside the active region; it consists of 41 images over a time interval of about 40 minutes (17:10 - 17:50 UT). The field of view of the THEMIS images used in the present

analysis is 35×35 arcsec.
Along with the raw data, we took 20 dark current images and 40 sequences of flat field images (pointing to a solar region characterized by opposite longitude in respect of AR 9445). The flat field images were acquired while the telescope was executing an ellipse.
In order to obtain corrected images from the raw images we have used the following reduction method:

$$I^{Cor} = \frac{I^{Raw} - < dark >}{< flat > - < dark >}, \tag{1}$$

where I^{Cor} is a corrected image, I^{Raw} a raw image, $< dark >$ is the average of all dark current images and $< flat >$ is the average of all flat field images at the wavelength of the raw image to analyse.
The images have been filtered by means of a WIENER Filter to reduce seeing noise and to improve the image quality. Seeing conditions were such that a spatial resolution of ~ 0.8 arcsec was achieved.

3. Data Analysis

NOAA AR 9445 arrived at the east limb on April 29, 2001 (its average latitude was about 25N) and departed over the west limb on May 10, 2001.
Fig. 2 (a,b,c) shows the region on May 5, 2001 in white light (WL), Hα and 171 Å, respectively, and Fig. 2 (d) shows the active region's magnetic configuration. We can see that the active region has a large number of sunspots, a complex morphology with a $\beta - \gamma$ magnetic configuration, and that it appears to be very extended in longitude (longitudinal extension $\sim$ 27 heliographical degrees). In the Hα image acquired at 16:00 UT (Fig. 2 (b)) we can also note an elongated S-shaped filament, which coincides with the PIL and has a length of ~ 70000 km. The filament, in the region bounded by the box, appears to be wider than in the eastern part, but it is not bifurcated. Moreover, also Hα off-band images show only one single dark filament.

The 171 Å image shows the active region configuration at coronal level, where we can see that the EUV filament channel has a bifurcated shape (the analysis of 171 Å images indicates that the EUV filament channel began to show a bifurcated shape at $\sim 15:30$ UT).
In order to study the evolution of the filament, we have analysed the THEMIS and BBSO sets of chromospheric images: Hα center ($\lambda =$

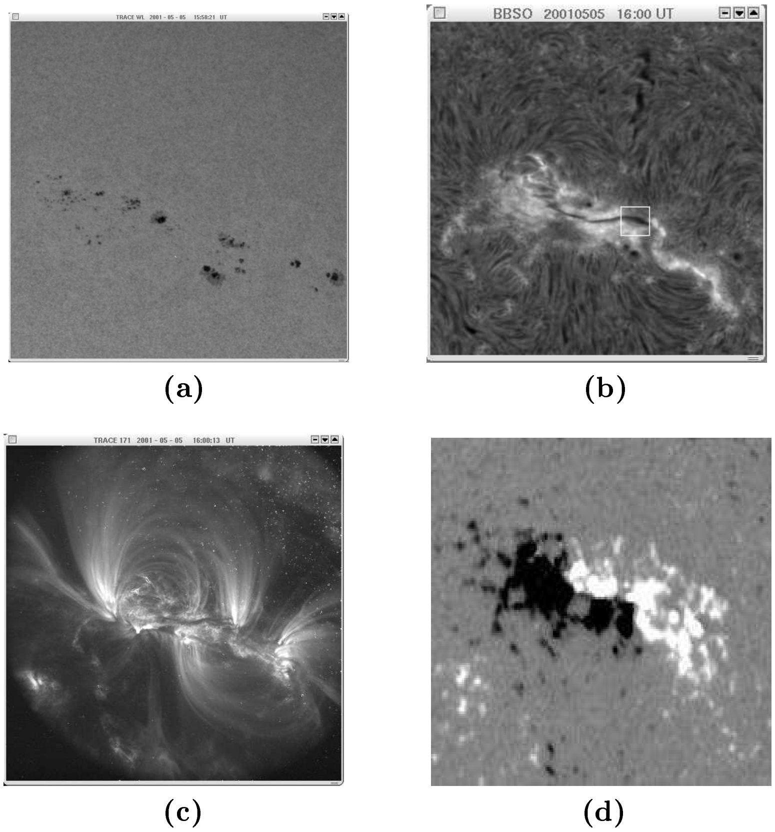

Figure 2. Images of AR 9445 on May 5, 2001: (a) TRACE WL image taken at 15:58 UT (fov $\sim$ 227500 $\times$ 227500 km^2); (b) BBSO Hα image taken at 16:00 UT (fov $\sim$ 245000 $\times$ 245000 km^2), the square indicates the field of view of THEMIS images; (c) TRACE 171 Å image taken at 16:00 UT (fov $\sim$ 358000 $\times$ 358000 km^2); (d) GONG magnetogram taken at 16:01 UT. In all the images north is on the top, west on the right.

6562.8Å), blueshifted (-0.50 Å) and redshifted (+0.50 Å).
Fig. 3 and 4 show the filament in the center of the Hα spectral line and in the line wings at five different times: 17:13 UT and 17:34 UT as deduced from the THEMIS observations; 18:01, 18:24 and 18:39 UT, as deduced from the BBSO data. In the left column we show the blue shifted images, in the center column the Hα center images and in the right column the red shifted images.
Data acquired by THEMIS at 17:13 UT show that the southern part of the filament appears broader in the red shifted images, indicating a downward plasma motion. Before the pre-flare phase, the filament slowly splits into two threads. The northern thread we marked by an A, the southern one by a B. These threads are better visible in the red

shifted images.
Moreover, all the images show a bright patch located where the filament bifurcates (arrow in the center column of Fig. 3 (b)). The area of the bright patch reaches the value of $\sim 4.9 \times 10^7 \;\; km^2$ when it extends in the east-west direction over 7000 km.
This bright patch was already visible in the first Hα image acquired at BBSO at 15:40 UT. It is therefore possible that it formed before the beginning of the observations. However, in the first available image it was only a little brighter than surrounding flocculi and there were several more like this. Moreover, the bright Hα patch (hereafter referred to as BHP) was not visible in Hα off-center images.
In order to check whether the BHP was the remnant of a small flare, we considered the flares occurred in this region and we found that two small flares occurred in the region only at 16:11 and 17:50 UT, respectively. Therefore the BHP observed at 15:40 UT should not be the remnant of a small flare.
Fig. 4 shows a sequence of BBSO images acquired during the pre-flare and main phases of the flare. In Fig. 4 (a) (center column), the

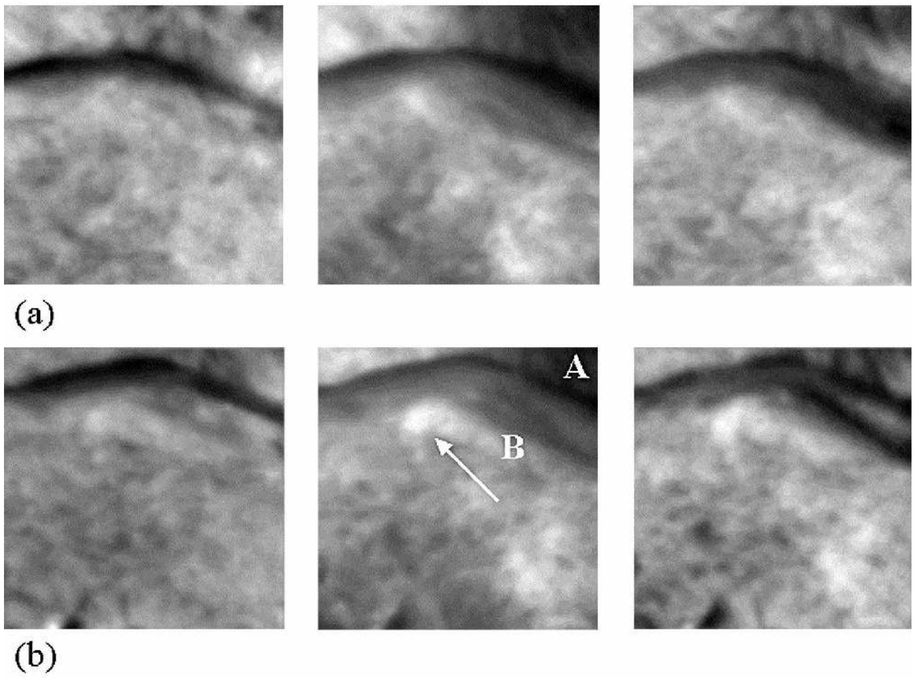

Figure 3. Sequence of blueshifted (left column), Hα center (center column) and redshifted (right column) images acquired by THEMIS at a) 17:13 UT, b) 17:34 UT. North is on the top, west on the right (fov $\sim 24500 \times 24500 \; km^2$).

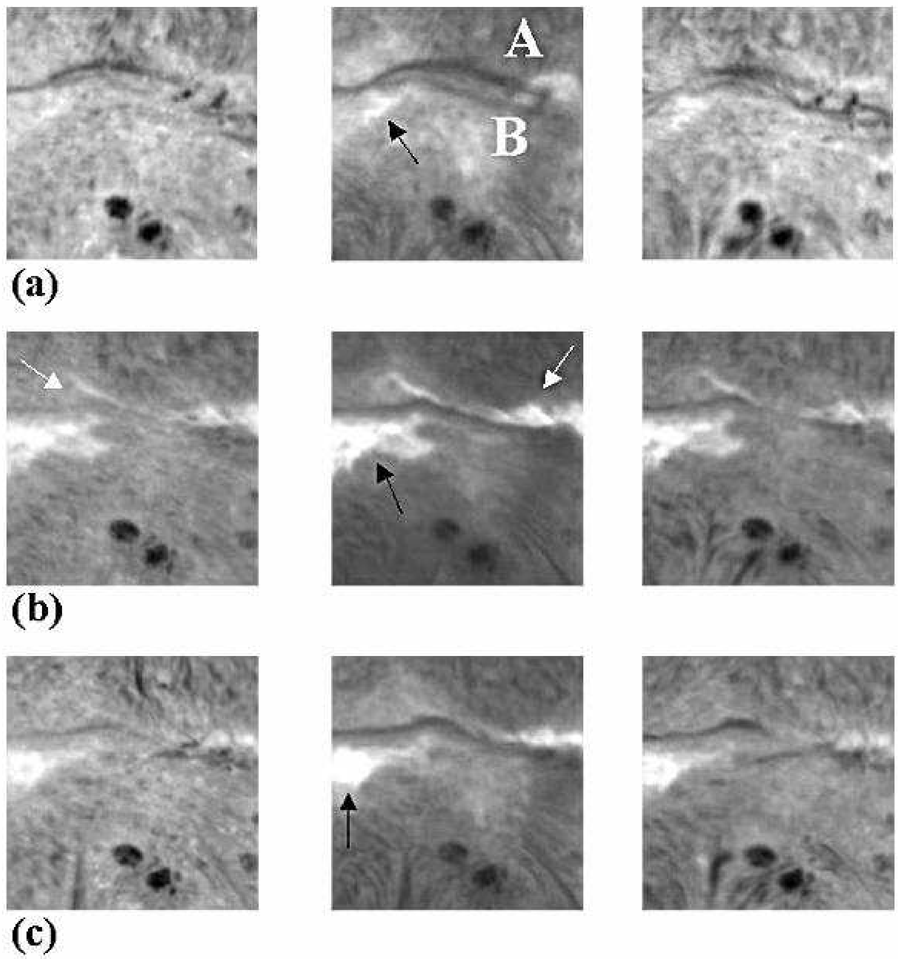

Figure 4. Sequence of blueshifted (left column), Hα center (center column) and redshifted (right column) images acquired by BBSO at a) 18:01 UT, b) 18:24 and c) 18:39 UT, respectively. North is on the top, west on the right (fov $\sim 40000 \times 40000$ km^2).

two threads, A and B, of the filament are still visible. Ten minutes before the flare peak the northern thread A erupted and an Hα ribbon appeared along the northern boundary of thread B (the white arrow in Fig. 4 (b)).

The location with stronger emission on the south of thread B initially coincides with the BHP visible in the THEMIS images (black arrows in the center column of Fig. 4 (a) and 4 (b)) and later shifts to the east (black arrow in the center column of Fig. 4 (c)). The distance between the centroids of the BHP and the south flare ribbon is ~ 6000 km.

Taking into account that both the Alfven speed and the speed of sound in the chromosphere are $\sim 7 \ \ km/s$, a wave disturbance or a horizontal conduction front would take ~ 15 minutes to travel that distance. Therefore it is difficult to establish whether the brightness increase in the south flare ribbon is due to a disturbance confined to the chromosphere, or to heating from coronal heights.

In order to detect motions in the filament before the flare, we obtained

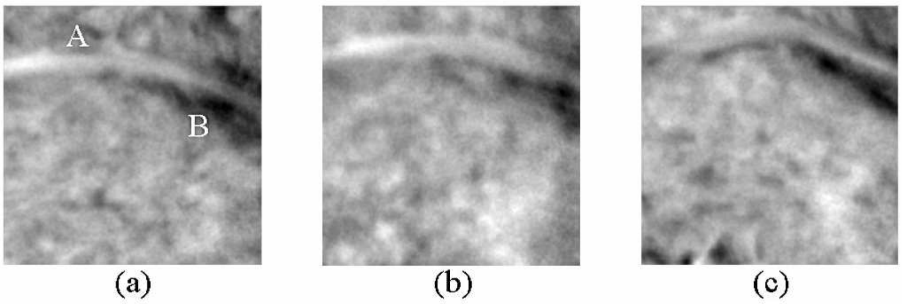

Figure 5. Line of sight velocity maps, obtained by subtracting THEMIS blue shifted images from red shifted ones, at a) 17:13 UT, b) 17:24 UT and c) 17:34 UT, respectively. White (black) areas indicate regions where upward (downward) motions are present. The fov of each image is $\sim 24500 \times 24500 \ km^2$.

line of sight velocity maps by subtracting blueshifted images from redshifted ones. Fig. 5 shows the velocity maps constructed from the THEMIS data at three different times. White (black) areas represent regions where upward (downward) motions are dominant.

One can see (Fig. 5 (a), (b)), that about one hour before the flare peak there is evidence of upward motions in the northern thread A of the filament. In Fig. 5 (c) upward motions are less pronounced. During the same period, the southern thread B moves downward (see Fig. 5 (a), (b), (c)).

Fig. 6 shows velocity maps obtained from the BBSO data in the pre-flare phase (18:01 UT) and during the main phase of the flare (18:24 and 18:39 UT), respectively.

At 18:01 UT the upward motion in thread A is less evident, while after the flare peak no upward motion is present. This indicates that thread A has already erupted.

In order to have a more complete scenario of the filament evolution, we report in Fig. 7 the morphology of the filament at four times : a) 16:41 UT on May 5, i.e. at a time preceding the filament eruption: we can clearly see thread A, while thread B is still very faint; b) 19:00 UT on May 5, after the eruption of thread A: we can see only thread B; c) 16:00 UT on May 6 : about 1 day after the eruption of thread A, we can see that the filament is no longer bifurcated and only one thread is visible; d) 15:00 UT on May 7 : 2 days after the eruption of thread A, the filament is only partially visible; however, there is a faint trace of one thread only.

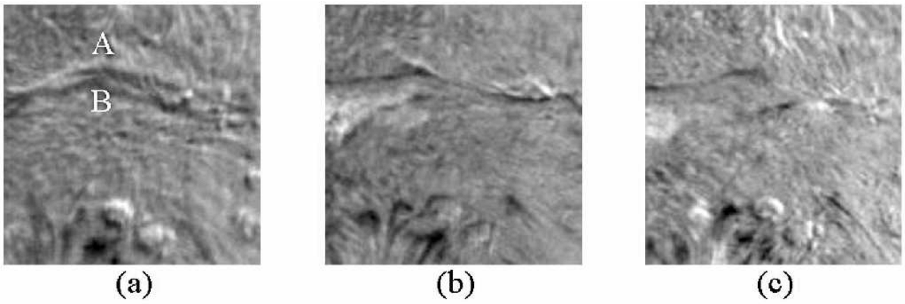

Figure 6. a), b), c) Line of sight velocity maps, obtained by subtracting blue shifted BBSO images from red shifted ones, at a) 18:01 UT, b) 18:24 UT and c) 18:39 UT, respectively. White (black) areas indicate regions where upward (downward) motions are present. The fov of each image is $\sim 40000 \times 40000\ km^2$.

As mentioned above, in the Hα center images (Figs. 3 and 4), a bright patch is located near the southern part B of the filament. This bright patch brightens and grows beside the bifurcation point of the filament.

From the analysis of the high resolution BBSO magnetograms we can infer that the BHP coincides with a positive polarity knot (PPK) of the magnetic field inside a more extended region of negative polarity (Fig. 8).

In order to determine whether this positive knot plays a role in the filament's destabilization, we have studied the evolution of its intensity and size. By studying BBSO magnetograms we found that the PPK is not yet clearly distinguishable on May 4, at 20:00 UT, while it is clearly visible on May 5, at 8:00 UT; moreover, after the flare onset, the size and intensity of the positive knot decreased. More precisely, the magnetic flux density in the knot increased from ~ 220 G to ~ 240 G until the filament erupted, then it decreased to 120 G at 19:50 UT. The PPK area decreased gradually from $1.4 \times 10^9\ \ km^2$ to $1 \times 10^9\ \ km^2$ during the interval 16:00 - 19:50 UT (see Fig. 9, where we also report the soft X-ray emission recorded by GOES during the period of interest).

We also followed the PPK evolution by using full-disk MDI magnetograms (high resolution MDI magnetograms of AR 9445 were not acquired on May 5). In Fig. 10 we show the PPK evolution, with a temporal cadence of two hours, as recorded by the MDI, from 00:00 UT to 22:00 UT on May 5. The arrows indicate, in each image, the location where the PPK emerged and evolved. We can see that the

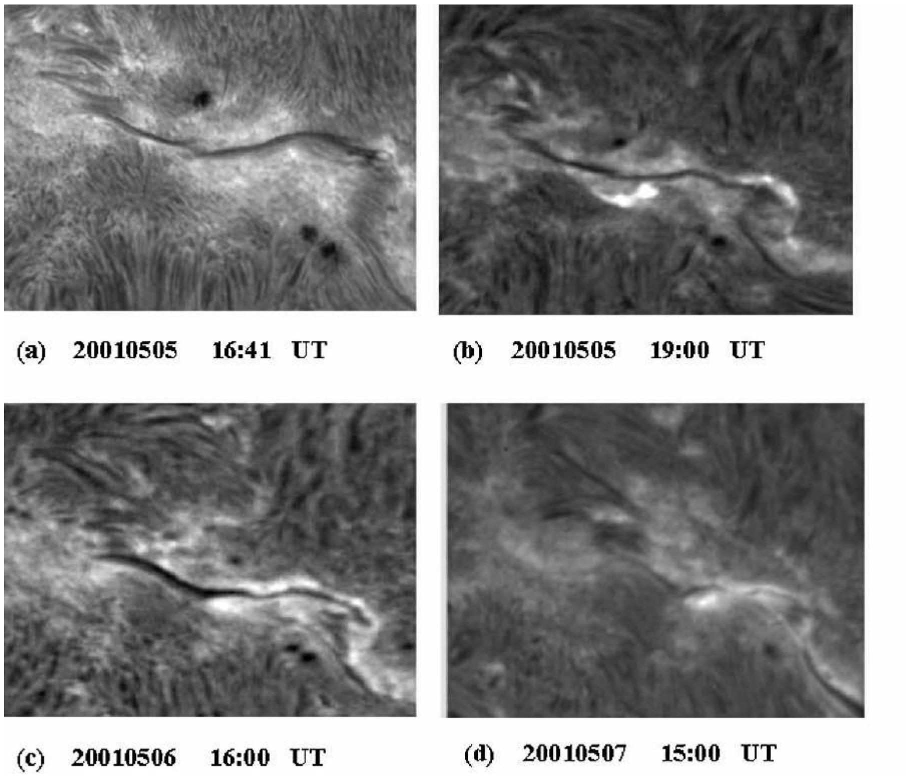

Figure 7. BBSO H_α images showing the morphology of the filament at four different times: (a) 16:41 UT on May 5; (b) 19:00 UT on May 5; c) 16:00 UT on May 6; d) 15:00 UT on May 7. North is on the top, west on the right. The fov of each image is $\sim 140000 \times 105000\ km^2$.

first clear evidence of the PPK emergence appears at 4:00 UT; then its area increases and the PPK is evident till 16:00 UT. After this time the PPK area quickly decreases and, by 22:00 UT, the positive polarity knot has disappeared.

Using BBSO high resolution magnetograms, we measured the local displacements of magnetic flux concentrantions between two successive magnetograms with the technique of local correlation tracking (November & Simon, 1988). In Fig. 11 we report the horizontal velocity fields in the photosphere obtained using the above mentioned method; the rms value of the horizontal velocity vectors has been found to be ~ 18 m s^{-1}. We found, during 16:00 - 17:00 UT, that the area where the PPK was located, was characterized by a rotational, clockwise motion, with an average velocity of ~ 120 m s^{-1}, as indicated by the black arrows superposed on the BBSO magnetogram. At the same time, in the region on the other side of the PIL there is indication of a likely

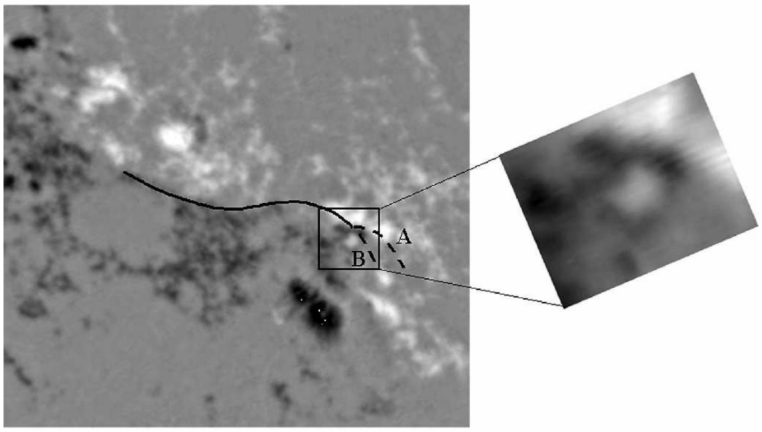

Figure 8. BBSO magnetogram of AR 9445 obtained on May 5, 2002 at 16:11 UT. White (black) represents positive (negative) polarity. The shape of the filament and the locations of threads A and B are drawn (fov $\sim 150000 \times 110000\ km^2$). The insert (fov $\sim 15000 \times 15000\ km^2$) shows an enlarged view of the PPK. North is on the top, west on the right.

compression of field lines toward the PPK.

Moreover, we analysed a sequence of the TRACE data taken at 171 Å. At 17:35 UT (Fig. 12 (a)) the TRACE filament, seen in absorption, is splitted in the same way as the Hα filament does. The site of the upper thread A of the filament brightens during the pre-flare phase (Fig. 12 (b)) (probably due to hot plasma rising with the erupting filament), while at the flare peak it dims (Fig. 12 (c)). During the main-phase of the flare it is possible to observe an increase of brightness in a loop-like structure which is apparently parallel to the EUV filament channel (Fig. 12 (d)). Later, the appearance of a greater loop-like structure, which seems to connect two regions on both sides of the EUV filament channel is observed (Fig. 12 (e), (f)).

We can exclude that this structure is the EUV signature of a surge because the high resolution BBSO Hα images acquired during the same interval of time do not show any surge in Hα, nor in Hα off-center images.

Considering the loop-like structures present in Fig. 12 (d), (e), (f), their different heights and the time delay between the eruption of the filament and their appearance ($\sim$ 20 and $\sim$ 50 minutes, respectively), we may presume that they are post-flare loops formed as a consequence of the reconnection of the loops of the arcade which were previously enveloping thread A. In particular, these loops become visible after that heat is dumped from a high-lying reconnection site, with consequent outflows of hot plasma, fast particles and conduction front, which prop-

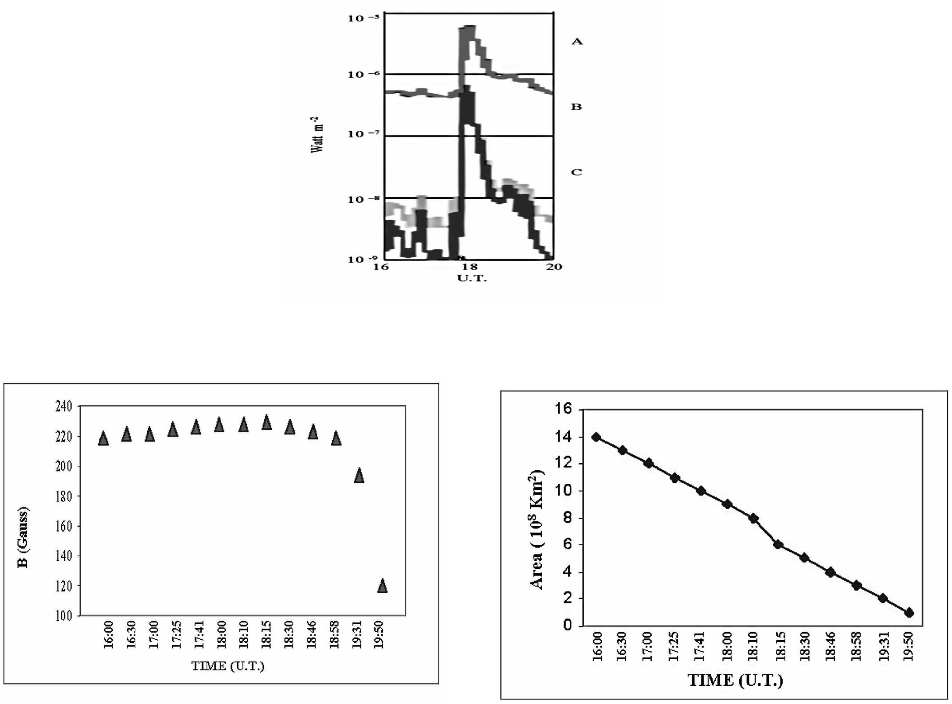

Figure 9. Top : Soft x-ray emission recorded by GOES satellite between 16:00 and 20:00 U.T.; bottom left : magnetic flux density variation in the PPK as deduced by BBSO magnetograms between 16:00 and 19:30 U.T.; bottom right : behaviour of the PPK area in units of $10^8\ km^2$ during the same time interval.

agate toward the footpoints and drive evaporation. The evaporating chromospheric plasma fills the loops with hot (several million degree) matter, not visible at 171 Å. When the loops cool down and drain, passing through the 171 Å regime, they become visible at this wavelength (Antiochos et al., 2000).
The post-flare loops visible in Fig. 12 (e), (f) have a length of $\sim 71000\ km$ and their eastern footpoints are anchored at a distance of $\sim 10000\ km$ from the bifurcation point observed in previous EUV images.

4. Summary of the Results

In summary, our analysis shows that the filament eruption on May 5, 2001 is characterized by the following elements:

- The filament seems initially to split into two threads.

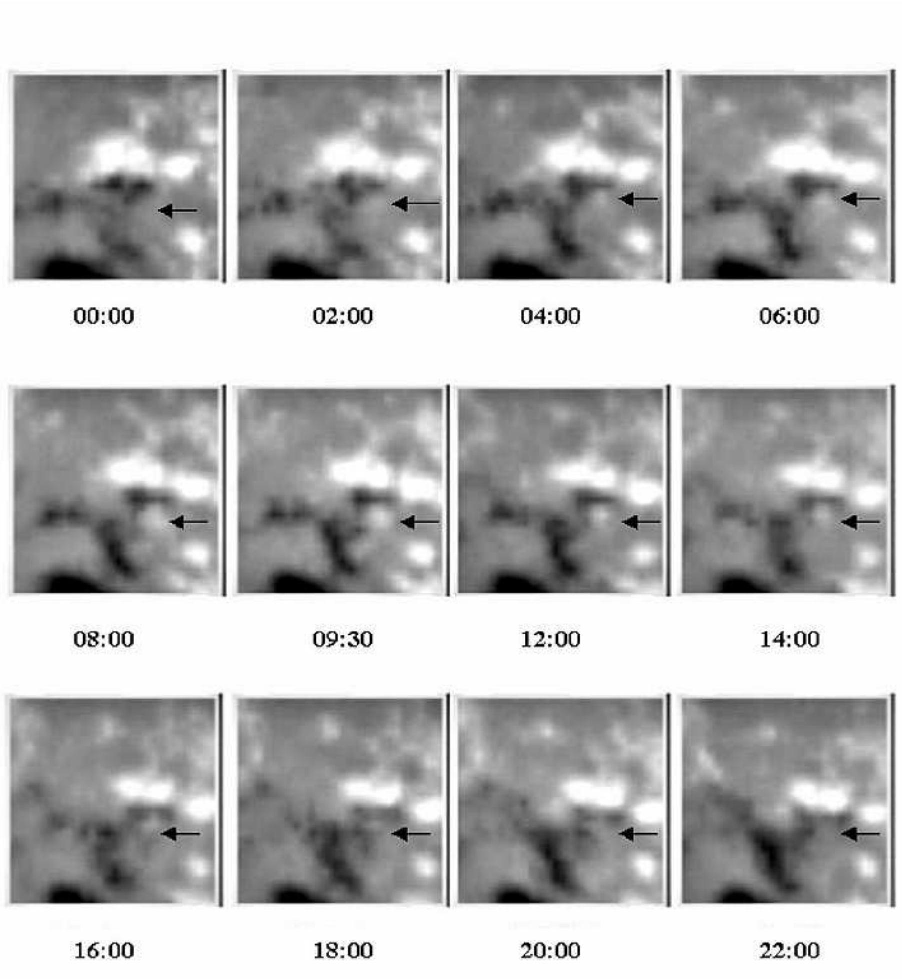

Figure 10. MDI magnetograms of the area where the PPK emerged and evolved. The arrows in each image indicate the PPK location. The fov of each image is $\sim 56000 \times 56000\ km^2$. North is on the top, west on the right.

- The southern thread B, formed as a consequence of a new magnetic field configuration, appears broader and better visible in redshifted images, indicating downward plasma motion.

- The northern thread A, which stays fixed with respect to the old PIL while the surrounding magnetic field configuration is changing, rises toward higher levels before the flare peak.

- A bright patch is visible, in Hα images, near the bifurcation of the filament, during the pre-eruption and the eruption phases; in this period it brightens and expands.

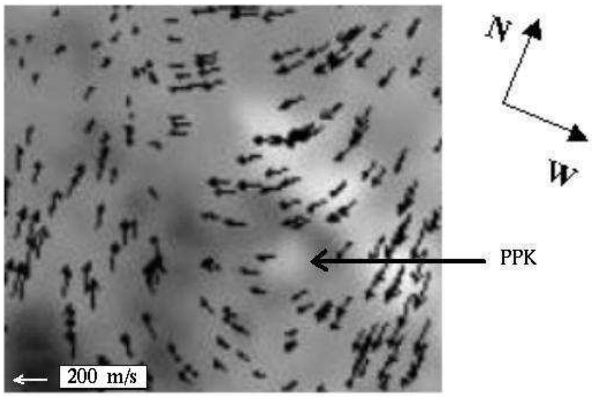

Figure 11. Superposition of the horizontal velocity field on the BBSO high resolution magnetogram of 16:00 UT (fov $\sim 11000 \times 11000\ km^2$).

- The bright patch observed in H_α images coincides with a positive knot of magnetic field inside an extended region of negative polarity. This positive polarity knot appears around 4:00 UT; it initially increases its area and intensity and later it quickly disappears.

- A map of the horizontal photospheric velocity fields indicate that during the formation of thread B, the site hosting the PPK presents a rotational flow; at the same time, a compressive flow toward the PPK is observed on the other side of the PIL.

- During the flare main-phase, EUV images taken at 171 Å show a loop system which was not previously visible: the eastern footpoints of the loop system are anchored at a distance of $\sim 10000\ km$ from the filament bifurcation point.

- After the eruption of thread A, the filament is no longer bifurcated; only one thread is visible for at least two days. The angular resolution and the temporal cadence of H_α images successive to 20:00 UT do not allow us to determine whether this thread coincides with the original thread A which reformed, or with thread B.

5. Discussion and Conclusions

On the basis of the observational evidences summarized in the previous section, we interpret the filament destabilization in AR 9445 in terms of a low-lying reconnection process between an old magnetic arcade supporting a filament and a new magnetic feature (NMF) of positive

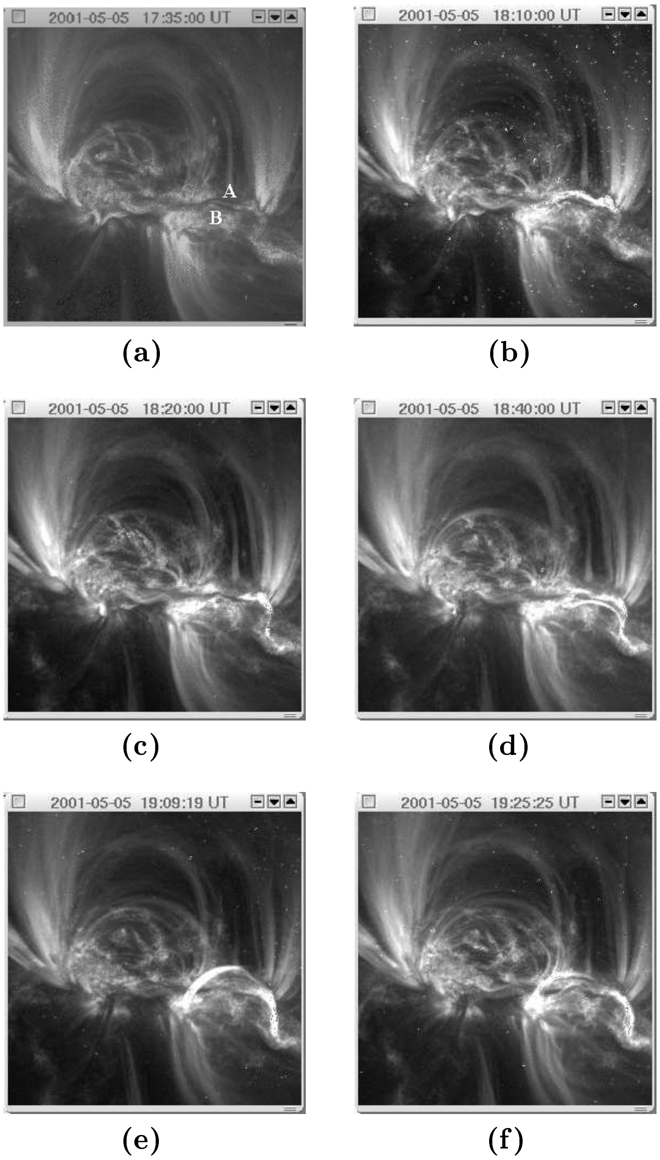

Figure 12. Sequence of 171 Å images taken by TRACE beetween 17:35 and 19:25 U.T., before, during and after the flare (fov $\sim 189000 \times 189000\ km^2$). North is on the top, west on the right.

polarity which appeared in an extended area of negative polarity.

We assume that initially the old arcade supporting the filament is characterized by a topology where the field lines sustaining the filament, which are the closest to the PIL, have a dip in their central part, while the farthest from the PIL are above the filament and contain it (Antiochos & Klimchuk, 1991).

The field lines of the NMF, located on the southern part of the filament (i. e. on the left of the main PIL), have opposite direction in respect of the arcade field lines.

The map of the horizontal velocity fields shown in Fig. 11 indicates that both the NMF and the region on the right of the PIL are characterized by motions which might have as a result the compression of the NMF field lines with the low arcade field lines. Therefore a magnetic configuration appropriate for a reconnection process between the new and the old flux in the low atmosphere may set in. Moreover, it appears from the MDI sequence shown in Fig. 10 that, between 4:00 and 14:00 UT, while the positive NMF flux strenghtens, the negative flux to its north side weakens: this last behaviour can be considered an indication of flux cancellation.

After the low-lying reconnection has taken place and the field line topology has changed, the filament appears to have split into two parts. It is difficult to establish why the new branch forms $\sim$ 12 hours after the appearance of the NMF; we suggest that there is this time delay because immediatelly after its first appearance, the new flux (which is mainly horizontal) cannot interact with the old coronal flux. A certain time is needed for the new flux to grow and expand outward until it reaches the old flux.

During the reconnection, part of the old magnetic flux supporting filament A has been cancelled by the NMF, leading to a potential catastrophe for the field supporting the filament. We stress however that the magnetic flux cancellation taking place between the NMF and the old magnetic flux is the most evident change in the active region configuration. Considering the numerous changes occurring in the AR magnetic configuration (see Fig. 10), we suggest that the eruption may be triggered by a concurrence of several factors. For instance, it is possible that the total mass of the filament supported by the main arcade has decreased and this decrease may cause a variation of the current intensity flowing in the filament. This phenomenon induces a loss of equilibrium between the forces (gravity force and Lorentz force) acting on the filament and, as outlined by other authors (see e.g. Vrsnak, 1990), when the ratio of the current intensity to the filament mass reaches a critical value, the filament eruption starts.

The eruption of thread A causes the appearance of the post-flare loops observed by TRACE at 171 Å from 19:09:19 U.T. (Fig. 12 (e)) to 19:25:25 U.T. (Fig. 12 (f)). When the filament thread A erupts, its rise towards the higher corona, causes a second reconnection at coronal levels, so that it is possible to observe these loops to brighten as a consequence of particle acceleration and heating from the high-lying reconnection site.

We therefore conclude that our observations may be interpreted in terms of a two-steps process. During the first step, a new magnetic feature appears near the PIL of an arcade sustaining a filament, the field lines of the NMF reconnect, in the low atmosphere, with the old arcade field lines; this reconnection creates a branch to a new filament channel and thread B forms. The second step is characterized by the loss of equilibrium of thread A, its eruption and the consequent breaking and reconnection of the arcade field lines above the filament.

We should have therefore observed two different processes of magnetic reconnection taking place in two different times and locations during the filament activation and eruption : a first low-lying, slow-mode reconnection occurring, at a low temperature ($T \sim 10^4 - 10^5\ K$), between the NMF and the arcade supporting the filament, which induces the filament destabilization and its rise toward the corona, and a successive fast reconnection taking place in higher arcade loops while the filament rises in the corona, and occurring at higher temperature ($T \sim 10^6 - 10^7\ K$).

Finally, we would like to mention that, as seen in MDI magnetograms, the NMF is not observed after 22:00 UT, indicating the cancellation of the PPK. Therefore it is possible that the western thread observed in H_α images successive to the event, might be due to the re-formation of thread A once the filament channel, formed by the PPK, had disappeared.

Acknowledgements

The authors wish to thank the referee of the paper (V. Gaizauskas) for his constructive comments. Thanks are also due to THEMIS staff for their efficient support in the observations, to TRACE team for their open data policy and the free diffusion of SolarSoftWare, and to BBSO staff for their continuous engagement in observations.

References

Amari, T., Luciani, J.F., Aly, J.J., Mikic, Z., Linker, J. ApJ, 585, 1073, 2003
Antiochos, S.K., Klimchuk, J.A. ApJ, 378, 372, 1991
Antiochos, S.K., Dahlburg, R.B., Klimchuk, J.A. ApJ, 420, L41, 1994
Antiochos, S.K., De Luca E.E., Golub L., Mc Mullen R.A. ApJ, 542, L151, 2000
Cavallini, F. A&A, 128, 589, 1998.
Gaizauskas, V. Sol.Phys., 121, 135, 1989.
Handy, B.N. et al. Sol.Phys., 187, 229, 1999.
Heyvaerts, J., Priest, E.R., & Rust, D.M. ApJ, 216, 123, 1977.
Kim, J.-H., Yun, H.S., Lee, S., Chae, J., Goode, P.R., Wang, H. ApJ, 547, L85, 2001
Martens, P.C.H. & Kuin, N.P.M. Sol.Phys., 122, 263, 1989
Martens, P.C.H. & Zwaan, C. ApJ, 558, 872, 2001
November, L.J. & Simon, G.W. ApJ, 333, 427, 1988
Priest, E.R., Forbes, T.G. Astron. Astrophys. Review, vol. 10, n. 4, 313, 2002
Smith, D.F., Hildner, E., Kuin, N.P.M. Sol.Phys., 137, 317, 1992.
Tandberg-Hanssen, E. *The Nature of Solar Prominences.* Kluwer Academic Publishers, Dordrecht, 1995.
Tarbell et al.. Proc. 3d SOHO Workshop, Solar Dynamic Phenomena and Solar Wind Consequence, ESA SP-373, 375, 1994.
Varsik, J.R., Sol. Phys., 161, 207, 1995
Vrsnak, B., Sol. Phys., 129, 295, 1990